Sensors and Materials, Vol. 26, No. 4 (2014) 253–262
MYU Tokyo

S & M 0989

Nondispersive Infrared Gas Sensor Using InSb-Based Photovoltaic-Type Infrared Sensor

Edson Gomes Camargo*, Seiichi Tokuo, Hiromasa Goto and Naohiro Kuze

R&D Center, Asahi Kasei Microdevices Corporation
2-1, Samejima, Fuji, Shizuoka 416-8501, Japan

(Received December 2, 2013; accepted February 17, 2014)

Key words: NDIR, InSb, photodiode, infrared, carbon dioxide, gas sensor

We have developed an uncooled InSb-based infrared sensor with small features, high sensitivity, fast response, and spectral response ranging from 2 to 7 μm. A miniaturized nondispersive infrared (NDIR) gas sensor module was also implemented and tested. Gas concentration measurements were performed, showing that the sensor can detect several gases, such as CO_2, CO, and NO_x, which have absorption peaks at the wavelength response range of the detector. In this work, a fully digital CO_2 meter was implemented, showing that our detector allows fast response measurements implementable in small modules.

1. Introduction

Mid- to far-infrared (IR) thermal-type sensors have been widely used in human body detection systems such as security and motion sensor lighting, in noncontact thermometry applications such as in-ear thermometers, and in several other consumer and industrial applications. They became popular because of its good responsivity at room temperature. On the other hand, conventional quantum-type detectors are known to have a higher signal-to-noise ratio (SNR) and fast response but require cryogenic cooling for operation, becoming more expensive than the thermal-type detectors.

With the mature experience of Asahi Kasei Microdevices (AKM) in III–V semiconductor-made Hall elements and other magnetic sensors, together with the above motivation to realize good-performance quantum-type IR sensors, the IR1011 was achieved. IR1011 is a very small uncooled InSb photodiode-based IR detector capable of detecting the far-infrared range, with competitive price and performance, when compared with conventional quantum-type detectors for the same wavelength range.

In this work, we report the basic characteristics of IR1011 and nondispersive infrared (NDIR) experiments using CO_2, CO, and NO_x gases showing its fast response, and also the performance of a fully digital CO_2 NDIR detection module with a gas cell having a 6-mm-long light path.

*Corresponding author: e-mail: camargo.eb@om.asahi-kasei.co.jp

2. Classification of Infrared Sensors

IR detectors are usually classified into thermal type and quantum type. As thermal-type detectors, pyroelectric sensors, thermopiles, and bolometers can be cited. Pyroelectric sensors are suitable and widely used for motion detection. In this type of infrared detector, IR light is absorbed by a piece of pyroelectric material such as PZT ($PbZrTiO_3$) or $LiTaO_3$, and during temperature variation provoked by light absorption, a consequent variation of spontaneous polarization occurs, resulting in a voltage output proportional to the rate of temperature variation. The signal is normally amplified by an FET, which is normally encapsulated together with the absorber in a can package for thermal insulation and electromagnetic noise shielding. Note that the output signal is obtained only when temperature variation occurs, which means that no continuous (or very low frequency) signals can be detected. For fast signals, responsivity has a trade-off with a cutoff frequency response, and will depend on the absorption coefficient, polarization rate and thermal conductivity between the absorber and the package.

Another popular type of thermal detector is the thermopile, which, thermally, has a similar structure to the pyroelectric sensor. Here, Bi or Sb is used to make hot bimetallic junctions to receive heat from the absorber and cold junctions, which must have a heat sink. The temperature difference will generate an output voltage according to the Seebeck effect, which occurs between the cold and the hot junctions. Micro-electromechanical systems (MEMS) technology is normally used in its fabrication, and rims are used to insulate the absorber and the hot junctions from the cold junctions. Instead of pyroelectric sensors, thermopiles are able to detect continuous irradiation while the temperature of the hot junction is different from the cold junction. However, the price-competitive thermopile's responsivity is still low, limiting its applications.

On the other hand, quantum-type detectors, which are made from a semiconductor material that determines its absorption wavelength, can operate very fast since the optoelectronic conversion is a fast process when compared with that of the thermal-type one. They are basically classified into photoconductors and photodiodes. For near-infrared or shorter wavelengths, reverse-biased photodiodes can provide a satisfactory SNR. The same does not occur for the mid- to far-infrared range, where narrow-bandgap materials (i.e., III–V compound semiconductors) are required. In these devices, $1/f$ noise markedly affects the SNR, and for this reason, photodiodes are normally operated in unbiased mode. To increase SNR to satisfactory levels, conventional III–V compound devices must be cooled with Peltier elements or cryogenic coolers.

Room-temperature-operable HgCdTe (MCT) devices have also been reported.[1–3] Although they have been used in military applications, mercury has been avoided in consumer applications.

InAsSb has also been reported, but Auger recombination processes are responsible for decreasing the performance of detector operation at room temperature.[4–7]

The IR sensor described in this work is based on several barrier-type photodiode structures connected in series,[8] which allows room-temperature operation with good SNR for human body detection, thermometry, and also NDIR gas sensing.

3. AKM's InSb-Based Infrared Sensor

3.1 *Sensor structure*

AKM's infrared sensor (IR1011) is fabricated starting with a mature epitaxy of InSb single crystal on a semi-insulating GaAs substrate by molecular beam epitaxy (MBE). The cross section and band diagram of the photodiode structure are shown in Fig. 1. The structure consists of a Sn-doped n-InSb layer, followed by a Zn-doped i-InSb layer, a p-AlInSb barrier layer, and finalized with a Zn-doped p-InSb top layer. The AlInSb barrier layer forms a potential barrier, which reduces the diffusion of excited electrons at the conduction band.

The *I-V* characteristic of this structure was compared with that of a conventional InSb photodiode without a barrier layer, and a remarkable decrease in reverse current was observed.[9–10] This result is supposed to be mainly due to the decrease in the rate of current diffusion to the p-InSb layer of excited electrons in the conduction band, which also increases the resistance under near-zero bias condition. Figure 2 shows the dark *I-V* curve of a photodiode with 9 × 9 μm² junction area measured at a temperature of 300 K. Note the good rectifying characteristics even at room temperature. The final detector consists of several single photodiodes with i-layer thickness of 2 μm connected in series,

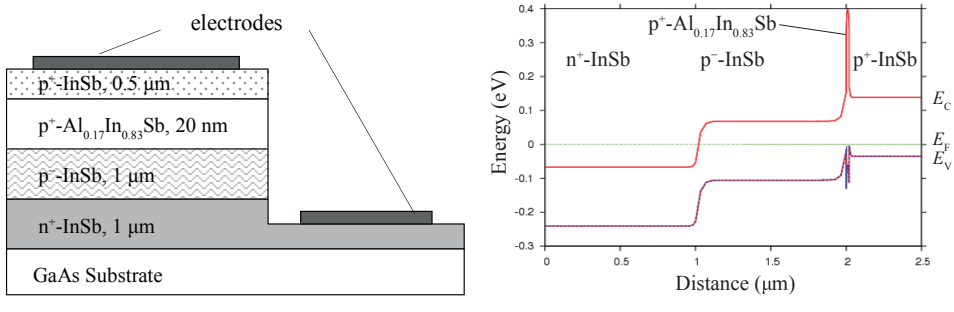

(a) (b)

Fig. 1. Cross section (a) and energy band diagram (b) of a single InSb photodiode.

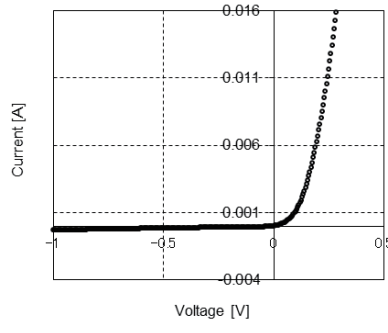

Fig. 2. *I-V* curve at 300 K of InSb photodiode with 9 × 9 μm² junction area.

which is necessary to increase the impedance and improve the SNR when connected to conventional preamplifiers. The total chip size is 700 × 700 μm^2 and 396 photodiodes were connected in series giving us a total nonbiased impedance of 150 kΩ, at room temperature.

3.2 *Specifications*

Since IR1011 does not require hollow regions to thermally insulate the absorber region, it can be encapsulated in a plastic mold, becoming very small in size. As shown in Fig. 3, IR1011's package consists of a 2.7 × 1.9 × 0.4 mm^3 small outline nonleaded (SON)-type molding, which can easily be soldered in a printed circuit board (PCB).

On the surface of the package, the backside of the GaAs wafer, which is coated with an oxide protection layer, becomes the light incidence window of the device.

The device was optimized for best SNR when connected to a transimpedance preamplifier, showing a typical nonbiased resistance of 150 kΩ and a typical output current of 6 nA, when placed at a distance of 100 mm from a 500 K blackbody, with an aperture of 22.2 mm diameter.

3.3 *Responsivity*

A 500 K cavity blackbody equipped with a wheel chopper was used as a light source, and responsivity measurements were performed at room temperature. Figure 4 shows the responsivity and Fig. 5 shows the noise equivalent power (NEP), both as functions of chopping frequency for the IR1011 and conventional thermal-type detectors (thermopile: Perkin Elmer TPS434, pyroelectric: Nicera RE210). The sensor responsivity, which was calculated from the output obtained from the total light power in the whole area occupied by the photodiodes, was almost the same as that of the pyroelectric, around the frequency of 8 Hz and kept constant for signals ranging from DC to 500 Hz, which confirms its static and high-speed operation. The voltage generated in the pyroelectric sensor disappears when no thermal variation occurs. For this reason, it is not able to output a DC voltage when detecting constant or low-frequency signals. Moreover, since its output depends on the temperature variation rate of the pyroelectric element after IR absorption, its responsivity is lowered at high chopping frequencies.

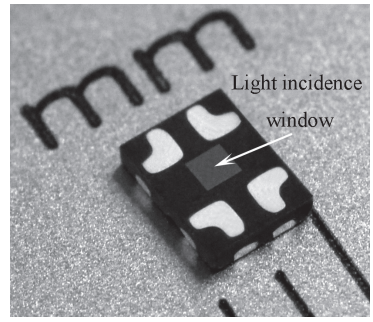

Fig. 3. AKM IR sensor (IR1011).

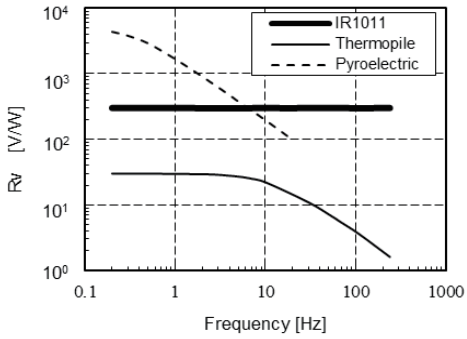

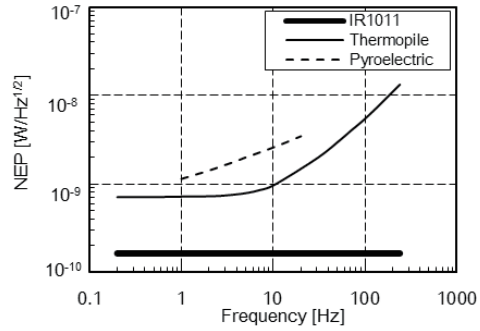

Fig. 4 (left). Responsivity vs frequency.
Fig. 5 (right). NEP vs frequency.

The IR1011 was immune to external thermal fluctuations or other noise sources, giving us a typical detectivity (D^*) of 2.8×10^8 cm·Hz$^{1/2}$/W for a single photodiode at room temperature.

3.4 *Spectral response*

Spectral response was measured using a monochromator equipped with a ceramic heater light source and chopper. An IPHT TS-100 thermopile, whose output has a flat response in a wide wavelength range, was used as reference. IR1011 and the reference thermopile outputs were measured at a chopping frequency of 1 Hz, with a 35670A Dynamic Signal Analyzer, and the absolute responsivity as a function of wavelength was obtained. Figure 6 shows the spectral response measurement result for the IR1011, which showed peak responsivities of 5 and 6 μm and a cutoff wavelength of 6.8 μm.

At lower wavelengths, the responsivity is supposed to be limited by the GaAs substrate transmittance, with a cutoff wavelength of approximately 1 μm. These results show that the IR1011 can be used for NDIR detection of several environmental gases, as will be discussed in the next section.

4. NDIR Gas Detection Using IR1011

4.1 *NDIR gas detection*

The transmission spectra of several gases and water are shown in Fig. 7. Here, we can see that in the 3–7 μm range, the main environmental gases (*e.g.*, CO_2, CO, NO, and CH_2O) have distinct absorption peaks.[11] As shown in Fig. 6, the IR1011 spectral response fits to the NDIR detection of all those gases, and selectivity can be acquired using band-pass filters (BPFs) tuned to the corresponding absorption wavelength for each gas (*e.g.*, CO_2: 4.3 μm, CO: 4.6 μm, NO: 5.4 μm, and CH_2O: 5.6 μm).

In an NDIR gas sensor, the gas concentration can be obtained on the basis of the Lambert-Beer law shown in eq. (1).

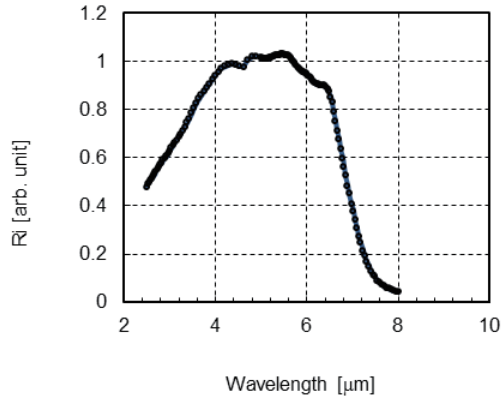

Fig. 6. Spectral response of IR1011.

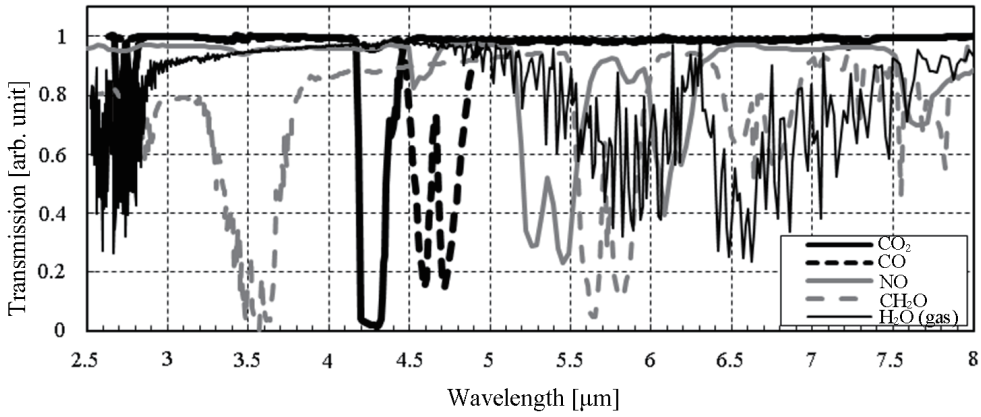

Fig. 7. Transmission spectra of several gases and H_2O.[11]

$$\mathrm{Log}(T) = \varepsilon \cdot c \cdot l \tag{1}$$

Here, T is the transmittance, ε is the absorption coefficient, l is the cell length, and c is the gas concentration.

As shown in Fig. 7, there is no absorption by H_2O or other gases in the 3.9 μm wavelength. This is the reason why this wavelength is normally used as reference in conventional NDIR sensors. In a 2-wavelength-channel NDIR system, one can calculate the gas concentration based on eq. (1) by taking the logarithm ratio of the main sensor signal (i.e., with BPF tuned to the gas absorption wavelength) to the reference sensor signal (i.e., with BPF tuned to 3.9 μm) and adding a constant that depends on system design, such as lamp output power, cell loss, etc.

4.2 *Measurement results*

Figure 8 shows the NDIR experimental apparatus. It consists of a gas cell, with a filament lamp coupled on one side and a PCB on the other side. The PCB contains two IR1011 packages, one with a 3.9 μm BPF and the other with a BPF corresponding to the absorption peak of the gas to be detected.

Figure 9 shows the sensor output as a function of CO_2 concentration, for 20- and 40-mm-long gas cells, which were obtained using a Telaire 7001 CO_2 meter. A BPF with center wavelength of 4.26 μm and bandwidth of 180 nm was used for the CO_2 channel, and for the reference channel, a BPF centered at 3.9 μm with a bandwidth of 156 nm was used.

The output axis was obtained from the ratio between the reference channel and CO_2 channel outputs. Note that for 0 ppm concentration, the curve does not cross the origin, but some offset value, which represents the ratio of the logarithm of the two output channels, when light is not absorbed.

To verify the response speed of the system, a mixture with a CO_2 gas concentration of about 2000 ppm was suddenly inserted into the cell, followed by a sudden purge with fresh air (400 ppm). The response signal for CO_2, which was converted to gas concentration, is shown in Fig. 10. From these results, not only fast response, but also a high SNR can be observed.

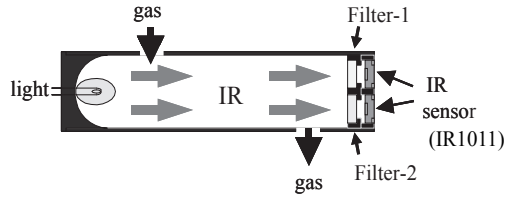

Fig. 8. Gas cell structure.

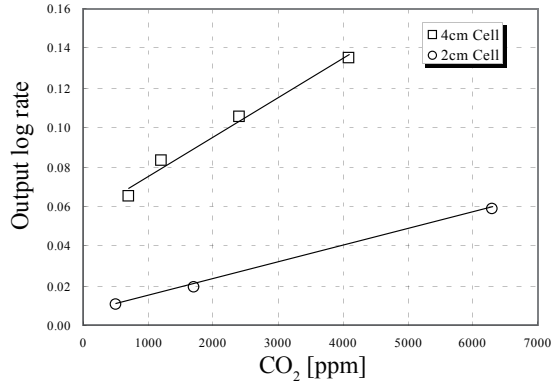

Fig. 9. Sensor output as a function of CO_2 concentration.

In a similar way, output signals equivalent to a response to 100% concentrated CO and NO_x were obtained, as shown in Figs. 11 and 12, respectively. Here, the gas-measurement channel filter was changed to filters with a center wavelength of 4.66 μm (bandwidth of 80 nm) for CO and 5.15 μm (bandwidth of 370 nm) for NO_x.

A slight signal decrease (Figs. 10 and 11) after gas insertion was observed in the above experiments using CO_2 and CO. This is supposed to be due to the concentration decreasing during gas spreading. The response for NO_x showed a different behavior, as shown in Fig. 12, from the results shown in Figs. 10 and 11. The reason for this behavior is under investigation.

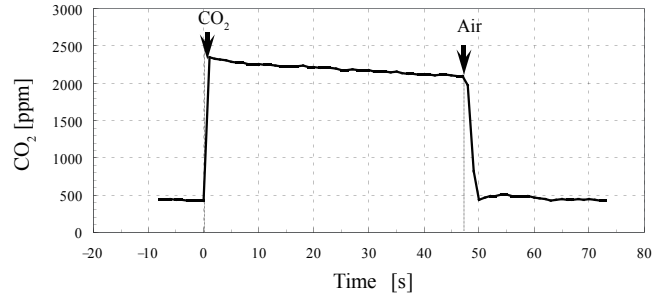

Fig. 10. Sensor response to CO_2 converted to CO_2 concentration.

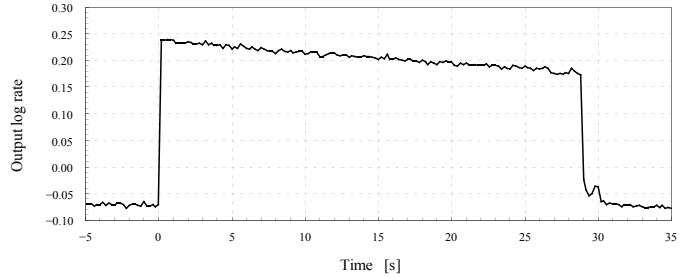

Fig. 11. Sensor response to CO.

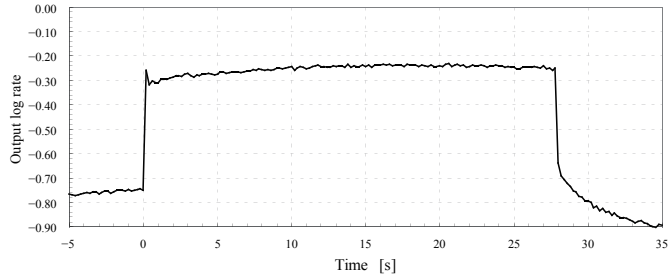

Fig. 12. Sensor response to NO_x.

5. CO_2 NDIR Module

A practical, fully digital, maintenance-free CO_2 miniaturized module, with a I2C serial output interface was implemented (see Fig. 13). The specifications are shown in Table 1.

The module includes a gold-coated gas cell with a 6 mm light path length, which allows its miniaturization. During one measurement cycle, the lamp must be turned on for 200 ms. At 3 V power supply and measurement cycle of 2 s, the power consumption was as low as 3 mW on average. Moreover, a PC interface circuit (Fig. 14) was used for long-term data logging, which showed very good stability. The module shown in Fig. 13 is suitable for several applications, such as cabin air monitoring in vehicles and building air conditioning systems. Moreover, the small features and low power consumption allow the module to be used in battery-powered or portable equipment, such as mobile devices.

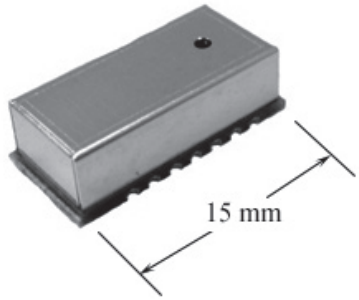

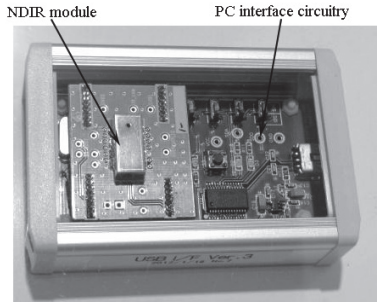

Fig. 13 (left). CO_2 NDIR module (light path length: 6 mm).
Fig. 14 (right). CO_2 NDIR module including PC interface circuitry.

Table 1
Specifications of CO_2 measurement module.

Size	15 × 7 × 4.5 mm^3
Supply voltage	2.7–5.5 V
Power consumption (@ V_{dd} = 3 V, 8 s/measurement)	3 mW
Sensitivity range	300–5000 ppm
Operation temperature	0–50 °C
Interface	I2C

6. Conclusions

We have developed a very small featured InSb-based infrared sensor with spectral response ranging from 2 to 7 μm. NDIR gas sensing was performed using CO_2, CO, and NO_x gases, showing a fast and stable response with satisfactory SNR. A miniature fully digital, low-power-consumption module with I2C output was also implemented, showing stable operation for environmental CO_2. With these results, it was demonstrated that by using the AKM's IR1011 as an IR detector, very small systems with very low power consumption and a cost-competitive system can be implemented, allowing wider market spread in the future.

References

1 J. Piotrowski and W. Gawron: Infrared Phys. Technol. **36** (1995) 1045.
2 J. Piotrowski and M. Razeghi: Proc. SPIE. **2397** (1995) 180.
3 P. Martyniuk and A. Rogalski: Opto-Electro. Rev. **21** (2013) 239.
4 J. D. Kim, S. Kim, D. Wu, J. Wojkowski, J. Xu, J. Piotrowski, E. Bigan and M. Razeghi: Appl. Phys. Lett. **67** (1995) 2645.
5 J. D. Kim and M. Razeghi: Opto-Electron. Rev. **6** (1998) 217.
6 M. Razeghi: Opto-Electron. Rev. **6** (1998) 155.
7 T. Ashley, A. B. Dean, C.T. Elliott, C. F. McConville, G. J. Pryce and C. R. Whitehouse: Appl. Phys. Lett. **59** (1991) 1761.
8 N. Kuze, E. G. Camargo, K. Ueno, T. Morishita, M. Sato, M. Kurihara, H. Endo and K. Ishibashi: J. Cryst. Growth. **301**–**302** (2007) 997.
9 N. Kuze, E. G. Camargo, K. Ueno, Y. Kawakami, Y. Moriyasu, K. Nagase, M. Sato, K. Ishibashi and M. Ozaki: Phys. Status Solidi C **3** (2006) 431.
10 K. Ueno, E. G. Camargo, Y. Kawakami, Y. Moriyasu, K. Nagase and N. Kuze: Mater. Res. Soc. Symp. Proc. **891** (2006) 245.
11 NIST Chemistry Web Book (http://webbook.nist.gov/chemistry/).